Applied Radiation and Isotopes 225 (2025) 112077

Contents lists available at ScienceDirect

Applied Radiation and Isotopes

journal homepage: www.elsevier.com/locate/apradiso

Sensor performance evaluation for candidate photon readout systems in the RIPTIDE detector

Claudia Pisanti [a,b,*], Stefano Cecchini [b], Patrizio Console Camprini [c], Francesco Giacomini [d], Samuele Lanzi [a,b], Cristian Massimi [a,b], Alberto Mengarelli [b], Triestino Minniti [g], Agatino Musumarra [e,f], Maria Grazia Pellegriti [f], Alberto Piccioni [a], Riccardo Ridolfi [a,b], Roberto Spighi [b], Nicolas Terranova [c], Mauro Villa [a,b]

[a] Department of Physics and Astronomy, University of Bologna, Via Irnerio 46, 40126, Bologna, Italy
[b] INFN Bologna, Viale Berti Pichat 6/2, 40127, Bologna, Italy
[c] ENEA, Via Fermi 45, 00044, Frascati, Italy
[d] INFN CNAF, Viale Berti Pichat 6/2, 40127, Bologna, Italy
[e] Department of Physics and Astronomy, University of Catania, Via Santa Sofia 64, 95123, Catania, Italy
[f] INFN Catania, Via Santa Sofia 64, 95123, Catania, Italy
[g] Department of Physics, University of Rome "Tor Vergata", Via della Ricerca Scientifica, 1, 00133, Rome, Italy

ARTICLE INFO

Keywords:
Optical
Photons
Calibration
Sensor
RPTI
Scintillation
Imaging
Neutron
Detector

ABSTRACT

This paper describes a comparative study of three optical readout systems for the RIPTIDE detector, focusing on their performance under extreme low luminosity conditions. The systems analysed include the ASI533MM-PRO from ZWO, the ORCA-Quest2 from Hamamatsu, and an MCP-based setup built specifically. A key aspect of this analysis is the method to measure the intensity distribution of the diffraction peaks, produced by a coherent light passing through a single slit to study the photon sensitivity and the noise characteristics of the detectors. A photodiode detector for laser power measurement was used to quantify the total light intensity, which was then correlated with the grey level output recorded by each system. As expected, the results show that the ASI533MM-PRO exhibited lower photon sensitivity and higher background noise than the ORCA-Quest2, which demonstrated the capability of detecting single photons. The MCP setup, despite its higher background noise, benefited from light amplification, enabling detection of lower photon densities. This method of comparison provides a robust framework for evaluating the photon's detection sensitivity of optical readout systems for high-precision, low-luminosity applications like the RIPTIDE detector.

1. Introduction

RIPTIDE (Recoil Proton Track Imaging DEtector) is an innovative detector concept designed to track fast neutrons (Musumarra et al., 2021; Massimi et al., 2022; Camprini et al., 2023; Pisanti et al., 2024). It is based on the Recoil Proton Track Imaging (RPTI) technique (Wang and Morris, 2013), exploiting neutron-to-proton (n-p) elastic scattering to infer the neutron energy and direction from a measurement of the momentum of recoiling protons. The determination of the neutron direction is currently being investigated using different approaches (Mitchell et al., 2024; Marafini et al., 2017; Vanier et al., 2007), the most of them employing the RPTI technique.

A first prototype of the RIPTIDE detector has been assembled and is currently undergoing initial laboratory testing and characterization. It employs a $6 \times 6 \times 6\,\mathrm{cm}^3$ plastic scintillator, specifically polyvinyltoluene (material EJ-200, commercial equivalent BC-408), selected for its high proton density, H:C ratio = 1.104, and efficient light output, approximately 64% relative to Anthracene, with photon emission peaked at $\lambda = 425$ nm (Eljen Technology, 2021). This scintillator serves a dual purpose: acting as a neutron converter and as a charged particle detector. When neutrons interact elastically with protons within the scintillator, the resulting recoil protons produce scintillation light along their tracks. This scintillation light is captured using two orthogonal optical systems, both consisting of optical lenses and spatially-resolved light sensors, such as complementary metal–oxide–semiconductor (CMOS) cameras. Alternatively, Single Photon Avalanche Diode (SPAD) arrays, or TIMEPIX sensors can be used. The stereoscopic configuration enables

* Corresponding author at: Department of Physics and Astronomy, University of Bologna, Via Irnerio 46, 40126, Bologna, Italy.
E-mail address: cpisanti@bo.infn.it (C. Pisanti).

https://doi.org/10.1016/j.apradiso.2025.112077
Received 23 February 2025; Received in revised form 29 July 2025; Accepted 30 July 2025
Available online 7 August 2025

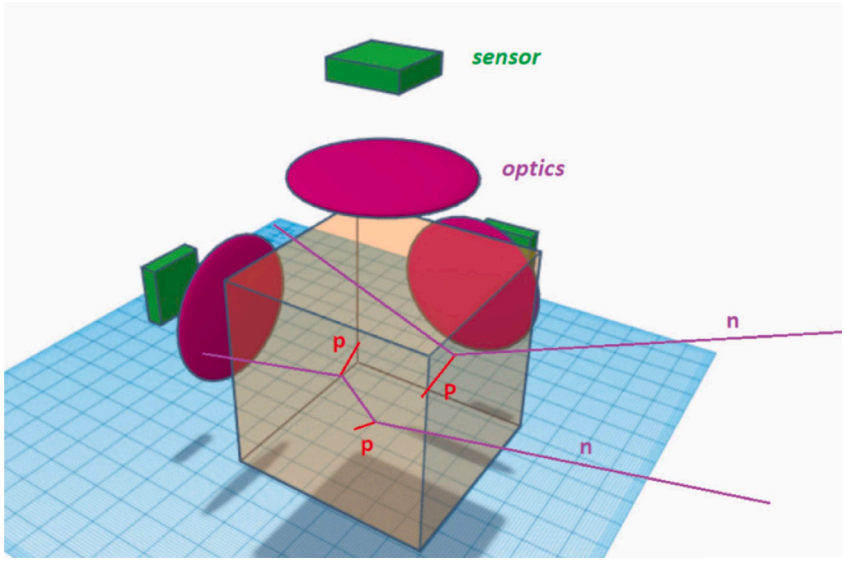

Fig. 1. A sketch of the RIPTIDE detector concept. A plastic scintillator made of polyvinyl-toluene is coupled to an optical readout system. The lenses are necessary in order to focus the scintillation light towards the optical sensors. Two optical readout systems are sufficient to obtain a three dimensional reconstruction of the track (Pisanti et al., 2024).

three-dimensional reconstruction of the proton tracks, thus enabling the determination of both the energy and direction of the incident neutrons.

The RPTI technique exploits the relationship between neutron and proton energy during elastic scattering, given by:

$$E_n = E_p / \cos^2(\theta) \tag{1}$$

where E_n is the neutron energy, E_p is the proton energy, and θ is the scattering angle. Therefore, by measuring the energy E_p and direction θ of the recoil proton, the energy E_n of the incident neutron can be determined, if the neutron direction is known. Additionally, if two consecutive n-p elastic scattering events are detected, both the energy and direction of the incoming neutron can be determined (Wang and Morris, 2013).

Monte Carlo simulations predict that the probability of detecting a single scattering event within the RIPTIDE detector is approximately 10%, while the probability of detecting two successive scattering events is around 1% for 20 MeV neutrons. A conceptual diagram of the RIPTIDE detector, illustrating its components and working principle, is presented in Fig. 1.

The main challenge of RIPTIDE is related to the extremely low amount of scintillation light produced by plastic scintillators, namely of the order of 10^4 photons/MeV. For instance, the spatial density of optical photons produced along the track by the passage of cosmic ray muons in a plastic scintillator like BC-408 is in the order of 10^3 photons/mm. Therefore, considering the tiny solid angle subtended by a single pixel, the number of photons reaching it is far below the readout noise.

To mitigate this situation, two primary approaches can be considered: (1) reducing the electronic noise of the readout system or (2) amplifying the photon signal through image intensification. The use of intensified cameras for particle track imaging has been used for more than fifty years (Stoudenheimer et al., 1960). Photon amplification using Microchannel Plates (MCPs) has been demonstrated to achieve gains as high as 10^6. Apart from commercial intensified cameras, other optical devices based on MCP-photon amplification can be found in the literature (Tremsin and Vallerga, 2020) and are currently under study. It is worth recalling that ultra-low-noise cameras, such as Hamamatsu ORCA-Quest2, have been employed for quasi-single-photon detection and imaging of scintillation light from particle tracks (Yamamoto et al., 2024), also for neutron detection (Yamamoto et al., 2023). The potential of SPAD-based cameras for this application is also under investigation (Bocchieri et al., 2024).

2. Photon detection systems

As already mentioned, the photon detection system must be capable of operating under extreme low-light conditions, necessitating (quasi) single-photon sensitivity, low noise, and high time resolution. Various sensor technologies were investigated, including:

- **ASI533-PRO MM (ZWO)** (ASI533-PRO MM, ZWO, 2022): containing a IMX533 Sony CMOS sensor with a resolution of 3008 × 3008 pixels and a 3.76 μm pixel size, this camera offers high quantum efficiency (80% at peak wavelength) and relatively low readout noise (1.0–3.8 electrons rms). It includes two-stage thermoelectric cooling capable of maintaining the sensor at −35 °C below ambient, which significantly reduces thermal noise. It can reach maximum 20 frames per seconds (fps) acquisition at full resolution. Despite the characteristics of this light sensor are not enough for RIPTIDE, it has been used as a control for the characterization performances of the camera.
- **ORCA-Quest2 (Hamamatsu)** (ORCA-Quest2, Hamamatsu, 2024): this innovative CMOS (qCMOS) sensor provides unprecedented performance with a resolution of 4096 × 2304 pixels and a 4.6 μm pixel size. It achieves a peak quantum efficiency of 85% (at 460 nm), ultra-low readout noise (0.30 electrons rms in ultra-quiet scan mode). The ORCA-Quest2 offers advanced photon-number resolving capabilities, making it ideal for low-light conditions. It supports up to 120 fps in standard scan mode and 25.4 fps in ultra-quiet scan mode at full resolution. Cooling options include forced-air or water cooling, enabling a sensor temperature up to −35 °C with a dark current as low as 0.006 electrons/pixel/s. Additionally, the camera is designed for seamless integration with external systems, featuring a variety of triggering options (edge, level, sync, etc.) with sub-microsecond precision.
- **Custom Intensified Camera (PHOTEK MCP** (Microchannel plate, PHOTEK, 2024) + **ASI533-PRO MM)**: This system integrates a Microchannel Plate (MCP) photon amplifier coupled to the ASI533 camera used in the first setup. The MCP has a large anode entrance (25 mm diameter), an alkali-based photocathode (S20) which offers broad spectral sensitivity with a quantum efficiency (QE) of 22% at the light emission wavelength of the BC-408 (~425 nm). The phosphor screen (P43) is made of Gd_2O_2S:Tb, with an efficiency up to 600 ph/e- at 10 keV, light emission

peaked at 545 nm, a decay time of less than 1 ms from 90% to 10% and 1.6 ms from 10% to 1%. The MCP features a typical quantum efficiency of 11.2% at 500 nm and radiant gain of $\leq 2.5 \cdot 10^5$ at 500 nm. This device is coupled to the ASI533 sensor through optics. The high gain of the MCP compensates for the ASI533 inherent noise. This combination provides a significant advantage in scenarios requiring photon multiplication under extremely low-light conditions.

The comparison and characterization of these sensors are described in detail in subsequent sections. Preliminary results indicate that each system presents specific advantages and limitations to address the stringent requirements of neutron detection in RIPTIDE. While the ASI533 is included in this study for comparison purposes, it is unsuitable for the intended application due to its high readout noise, which compromises its ability to detect weak scintillation signals. The ORCA-Quest2 stands out for its excellent quantum efficiency and ultra-low readout noise, making it highly effective in low-light environments. However, its frame rate is a limiting factor, particularly in experiments requiring high time resolution. The MCP system, when combined with fast frame-rate cameras, offers the potential for sub-millisecond scale time resolution. Nevertheless, its low quantum efficiency remains a concern, and further investigation is necessary to confirm whether the photon amplification mechanism sufficiently compensates for this limitation.

3. Preliminary test using radiation sources

As a first experimental test, we investigated whether it was possible to image the scintillation light from a plastic scintillator, specifically BC-408, using a commercial CMOS camera, i.e. the ASI533-PRO from ZWO mentioned above. The performances of this camera are excellent for deep-sky imaging thanks to the high sensitivity achievable with exposure times as short as few milliseconds. However, imaging scintillation light is very challenging.

As expected, it was not possible to image the scintillation light of cosmic muons. To increase the density of optical photons per unit length, sealed ^{137}Cs and ^{241}Am radiation sources with 10-μCi nominal activity were used. More in detail, the ^{241}Am radiation source presents an estimated activity of 353 kBq, mainly emitting a combination of 5.5 MeV α particles and 59.5 keV γ rays. Therefore, the scintillation light produced in the scintillator and acquired by the CMOS camera shown in Fig. 2 can be related to both radiation types. Also in these cases it was not possible to image single scintillation events. However, by increasing the exposure time of the CMOS camera, a clear evidence of the accumulated scintillation light was recorded. It is evident from Fig. 2 that the photograph of the scintillation light reproduces the geometry of the radioactive source structure.

Given the activity of the source and the exposure time of 1 s, it can be estimated that approximately 1000 α-particles were emitted in the scenario depicted in Fig. 2, a quantity significantly exceeding the requirements of the RIPTIDE detector. However, this preliminary and qualitative test allowed us – for the first time – to photograph the time-integrated scintillation light of a plastic scintillator using a commercial CMOS camera. On the other hand, from the same test it became evident that the choice of the readout system must be carefully considered. Quasi-single-photon counting detection needs to be achieved while acquiring at a fast frame-rate.

4. Sensor calibration and characterization

This section outlines the methodology employed to compare the performance of different optical readout systems.

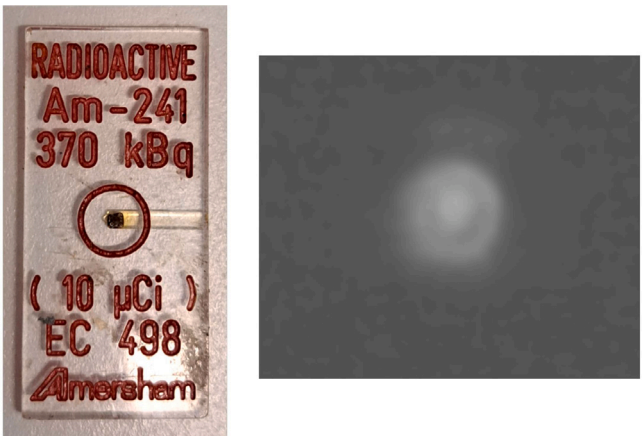

Fig. 2. Commercial ^{241}Am α-source used in the test and corresponding image of the time-integrated scintillation light recorded by the ASI533-PRO CMOS camera.

4.1. Materials and methods

It is well-known that when a coherent light passes through a narrow slit, it produces a diffraction pattern on a screen positioned at a large distance (i.e. Fraunhofer diffraction). The intensity distribution of light at the diffraction peaks is well-defined and follows the relation:

$$I(u) = I_0 \frac{\sin^2(u)}{u^2}, \qquad u = \frac{\pi}{\lambda} a \cdot \sin(\theta) \tag{2}$$

where I_0 is the intensity of the principal peak, λ is the wavelength of the light, a is the slit width, and θ is the diffraction angle.

Eq. (2) is valid for a monochromatic light, so that the incident light impinging on the slit can be assumed to have a planar wavefront, and the screen is assumed to be placed at a sufficiently large distance, approximately 30 cm from the slit in the present case. Although a narrow slit (adjustable mechanical slit VA100 Thorlab) of width 300 µm was used, we noticed that the light intensity across it was not as uniform as expected, thus creating some asymmetry in the diffraction pattern. This asymmetry was attributed both to the non-uniformity of the beam and to a slight misalignment in the experimental setup. Due to the sensitivity of the diffraction geometry, even small angular deviations between the laser, slit, and sensor planes were found to significantly affect the symmetry of the observed pattern.

In the diffraction pattern, the principal peak accounts for the majority of the diffracted light, approximately 90%, while the intensity decreases progressively for higher-order peaks. For instance, the second-order peak captures 2% of the total light, and the third-order peak captures 0.6%. Beyond these orders, the intensity rapidly diminishes, approaching negligible values.

Since the diffraction pattern distributes light across multiple peaks, significantly reducing the number of photons in each peak, this property makes it a valuable tool for evaluating the sensitivity of optical sensors. By analysing the detectability of progressively weaker diffraction peaks, the performance of optical readout systems can be characterized under low-light conditions. Therefore, the methods of diffraction was used to evaluate the sensitivity of the three optical readout systems mentioned above: the ASI533-PRO MM, ORCA-Quest2, and the Custom Intensified Camera. Although slightly different setups were required to accommodate the three sensors, all experiments utilized a laser-diode type PL205 from Thorlabs, having $\lambda = 405$ nm and a power of 0.9 mW.

Lasers-diodes, including PL205, exhibit non-uniform beam profiles, which violates the assumption of plane waves required by the diffraction model in Eq. (2). The assumption of uniform illumination was achieved using two different approaches, depending on the specific

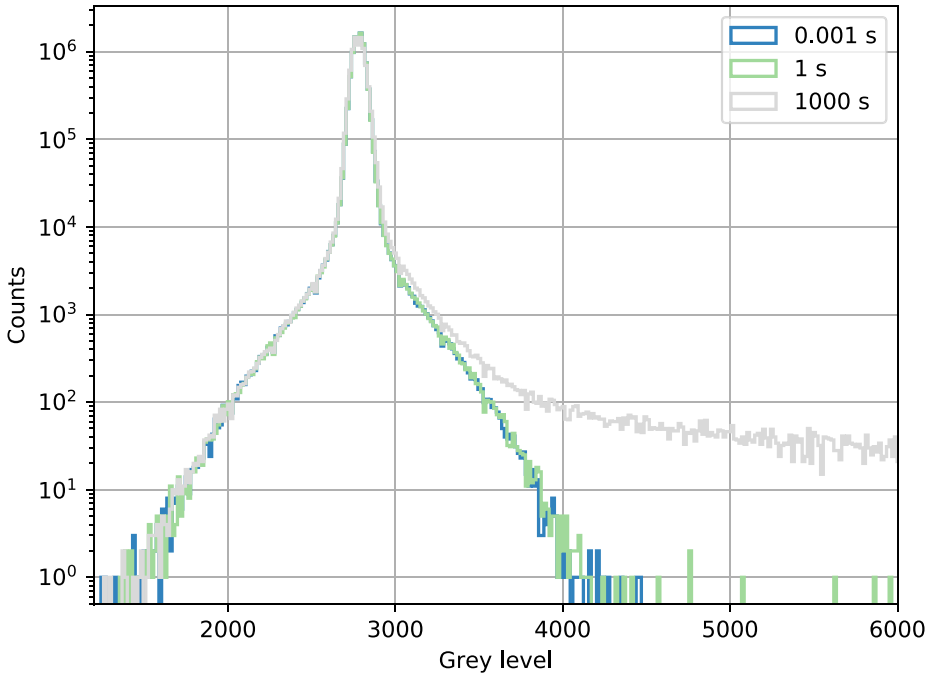

Fig. 3. Contribution of readout noise and dark current to total noise as a function of exposure time for a CMOS sensor.

setup: (1) enlarging the beam using a lens and isolating the central, flatter region with a diaphragm (Fig. 4, used with the ASI533MM-PRO setup) and (2) isolating the central portion of the beam using a pinhole (Fig. 5, applied to the MCP and ORCA-Quest2 setups). Although the second method produced a flatter and cleaner profile, diffraction artifacts from the pinhole were visible. The experimental setups were not identical, as each configuration was adapted to the specific requirements of the corresponding sensor. Nevertheless, these differences in setup did not significantly affect the outcome of the measurements.

Polarizers were used in all setups to reduce the laser intensity. For the MCP and ORCA-Quest2 setups, additional neutral density filters NE5-series from Thorlabs were employed to further attenuate the laser. Diffraction patterns were acquired at different exposure times: 1 ms for the ASI533MM-PRO, 199 ms for the ORCA-Quest2, and 500 ms for the MCP. The choice of exposure time and laser intensity for each system was based on the specific sensitivity and dynamic range of the detector. For each configuration, parameters were tuned to enable the detection of the maximum number of diffraction peaks without saturating the grey level in the principal peak. This strategy ensured a fair comparison of the systems' ability to operate under low-light conditions relevant to the RIPTIDE detector.

In CMOS cameras, the overall noise is typically described as the sum of two primary components: readout noise and dark current. Readout noise is an electronic noise introduced during the process of converting charge to digital signals in the camera readout electronics. This noise is largely independent of exposure time and is characterized in units of electrons root-mean-square (e^-RMS). Dark current, on the other hand, arises from thermally generated electrons within the sensor material during the exposure. Its contribution to the overall noise increases with both exposure time and the sensor temperature. To mitigate the effects of dark current, the CMOS sensor was operated with its cooling system engaged, and exposure times were minimized to limit the accumulation of thermally generated electrons.

Fig. 3 illustrates the contribution of readout noise and dark current to the total noise of different exposure times.

Fig. 6 shows the diffraction patterns obtained with the three systems. Notable differences include a horizontal pattern in the ASI533MM-PRO (Fig. 6(a)), attributed to the beam-flattening method, and visible noise from the MCP phosphor screen (Fig. 6(b)). Despite these differences, the diffraction patterns are evident in all the investigated setups.

To quantify the relationship between the total light exiting the slit and the grey-level intensity recorded by the optical readout systems, the photodiode detector PH100-Si-HA-OD1-D0 from Gentec-eo (Potentiometer Gentec-eo, 2024) was used for laser power measurement. The detector has a maximum average power of 300 mW, a noise equivalent power of 200 pW, a spectral range of 400–1080 nm, and the power calibration uncertainty is specified as ±5.0% for 400–419 nm. The aperture for the silicon sensor is 10 mm in diameter, enabling to integrate the laser light in a wide area, covering the full diffraction pattern.

This calibration process enables accurate mapping of the recorded grey levels to the actual light intensity, facilitating the evaluation of each optical system performance under varying conditions. Due to the photodiode sensitivity limitations, the custom intensified camera laser intensity was estimated indirectly by determining the neutral density filters' transmission and measuring the unfiltered laser intensity. The resulting intensities were 1.5 ± 0.1 μW for the ASI533MM-PRO setup, 0.20 ± 0.02 nW for the ORCA-Quest2, and 1.0 ± 0.1 pW for the MCP. For a known laser wavelength, the power intensities measured by the photodiode can be converted into integral number of photons reaching the photodiode.

$$n_{photons} = \frac{Power[J/s] \cdot Exposure\ Times\ camera[s]}{E_{photon}[J]} \tag{3}$$

4.2. Image analysis procedure

The acquired images were analysed using the following steps.

1. **Image rotation:** each diffraction pattern was rotated to align the primary axis horizontally, thus simplifying the area analysis. Nearest-neighbour interpolation was applied to minimize artifacts.
2. **Bias subtraction:** A bias value is typically added to the Grey level of all the cameras. This value needs to be estimated and removed to the image. In the case of the MCP, from Fig. 6(b), it is visible that the noise produced by the phosphor of the

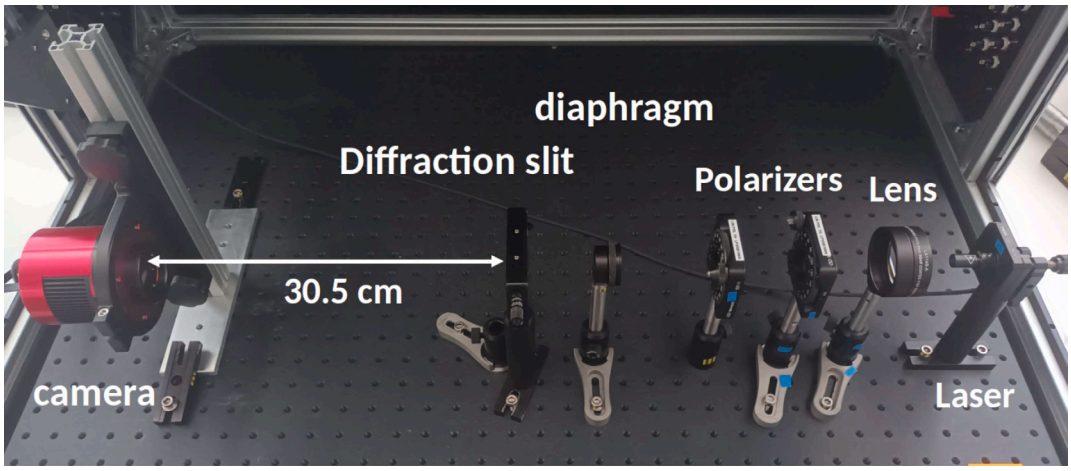

Fig. 4. Experimental setup for the ASI533MM-PRO setup utilized a lens and diaphragm to obtain a more uniform beam profile.

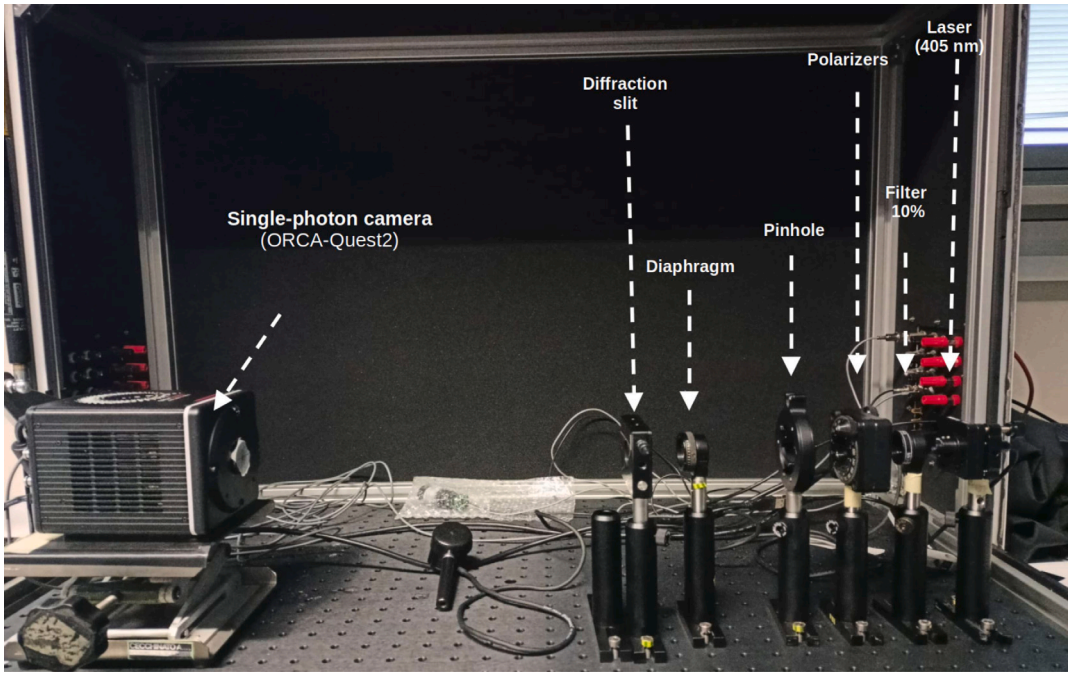

Fig. 5. Experimental setups for the ORCA-Quest2 and custom intensified camera employed a pinhole to isolate the central part of the beam.

MCP (the lighter circle in the picture) was higher than the bias of the ASI-camera (the darker part external to the circle), so the MCP background noise was estimated ad removed to the image together to the BIAS of the ASI-camera. To estimate the MCP background noise, an image region containing only the phosphor noise was selected, ensuring no contributions from signal photons. A histogram of Grey levels for the selected region was generated, and a Gaussian fit was applied to the data. From the fit, the mean (μ) and standard deviation (σ) of the noise distribution were extracted. The bias value to be subtracted from the image was determined as:

$$BIAS_{Customcamera} = \mu_{MCPnoise}. \quad (4)$$

This method ensured the systematic removal of the phosphor noise, allowing for a clearer analysis of the photon signal.

3. **Grey level to photon conversion:** Grey levels were converted to photon counts using calibration factors derived from the ratio of photodiode-measured intensity to total grey levels (Table 1).

Table 1
Photon-to-grey level conversion factors for the three systems.

ASI533MM-PRO	ORCA-Quest2	MCP setup
3.2 ± 0.2	0.133 ± 0.01	0.0039 ± 0.0004

4. **Diffraction pattern selection:** a horizontal slice was extracted from each image. Narrow slices (5 pixels) were used for the MCP and ORCA-Quest2 setups, while a broader slice (1200 pixels) was chosen for the ASI533MM-PRO to reduce uncertainty caused by horizontal artifacts. Fig. 7 shows the resulting diffraction pattern after photon to grey level conversion for the ORCA-Quest2 setup and for the custom intensified camera. To highlight the peak position, a convolution with a binomial and subsequently a uniform kernel of 10 pixel width was done (orange line).
5. **Peak identification.** Photon density at diffraction peaks was analysed and compared to system noise levels. Fig. 8 displays peak photon densities and noise thresholds for each system.

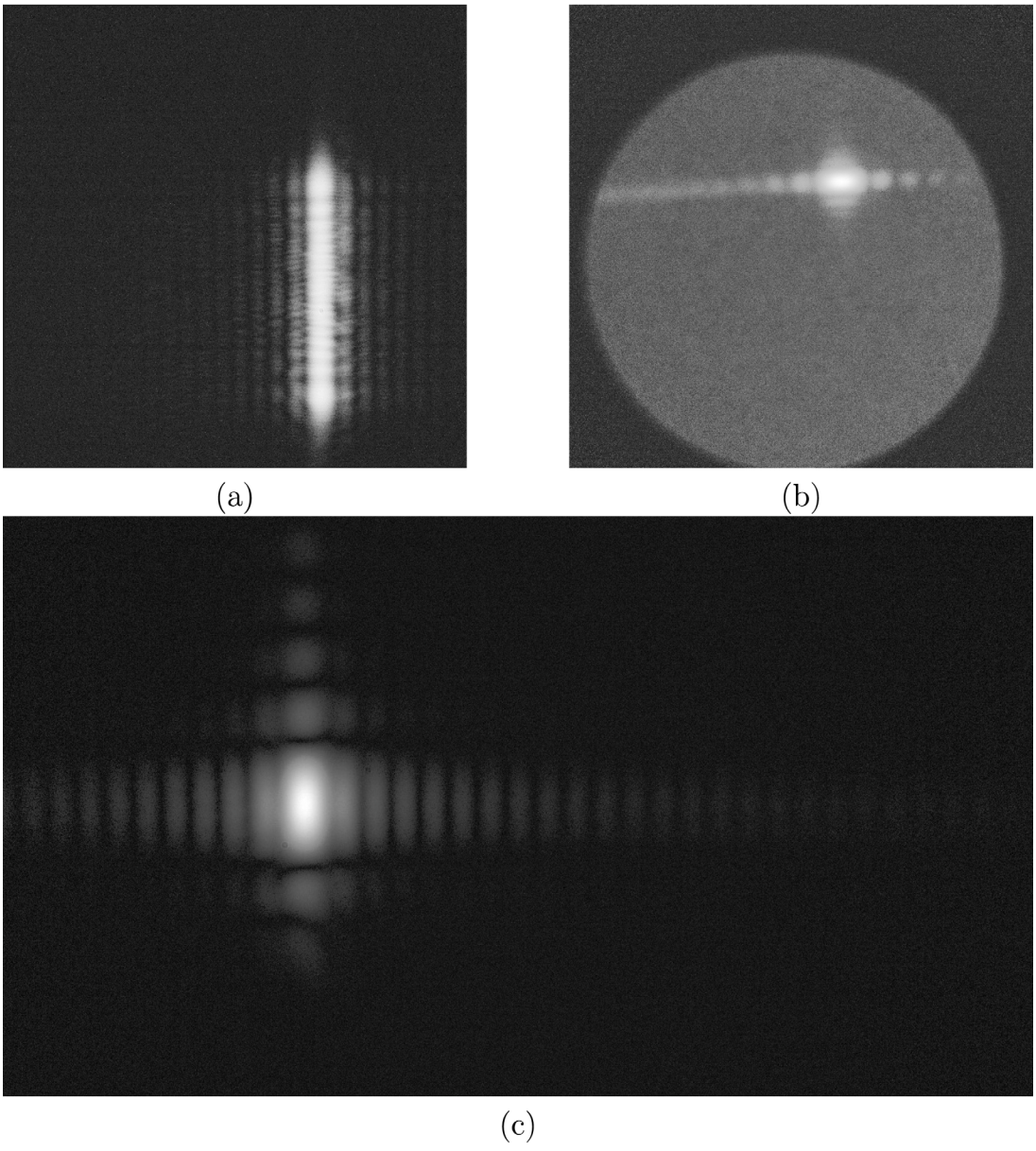

Fig. 6. Diffraction pattern obtained from the three systems. (a) ASI533MM-PRO (b) custom intensified camera, (c) ORCA-Quest2. The custom intensified camera setup highlights the circular phosphor screen, while the ASI533MM-PRO pattern shows horizontal features due to its beam-flattening method.

4.3. Results

Given RIPTIDE requirement to detect neutron events and accurately reconstruct proton tracks, the performance of the optical readout system – particularly in terms of noise levels, sensitivity, and photon density – directly influences the overall accuracy of determining neutron direction and energy. These parameters are critical for minimizing error rates in neutron trajectory reconstruction. Fig. 8 provides a direct comparison of the three optical systems. This visualization enables a clear assessment of their performance. The differences in diffraction peak intensities arise from variations in the experimental setup, while the discrepancies in noise levels are attributed to the intrinsic characteristics of the optical systems. To facilitate comparison, the same scale is used on the y-axis across all plots. As expected, the ASI533MM-PRO exhibited the lowest photon sensitivity and the highest background noise ($\pm$7.8 photons) among the three devices. The differences between the ORCA-Quest2 setup and the custom setup are more interesting. The ORCA-Quest2 exhibits lower camera noise, thus allowing to reach approximately one photon per pixel. All the peaks are clearly distinguishable. Conversely, the MCP setup exhibited background noise levels comparable to those of the ORCA-Quest2 ($\sim$0.27 photons/pixel vs. $\sim$0.33 photons/pixel respectively). However, the MCP photon amplification capability allowed it to detect lower photon densities.

In Fig. 6(b), the first three diffraction peaks are distinctly visible, while peaks up to the fifth order are identifiable despite reduced visibility. This corresponds to photon densities below 0.3 photons/pixel. While the ORCA-Quest2 excels in noise reduction and clear peak resolution, the MCP setup provides greater photon amplification, making it more suitable for scenarios involving extremely low light levels.

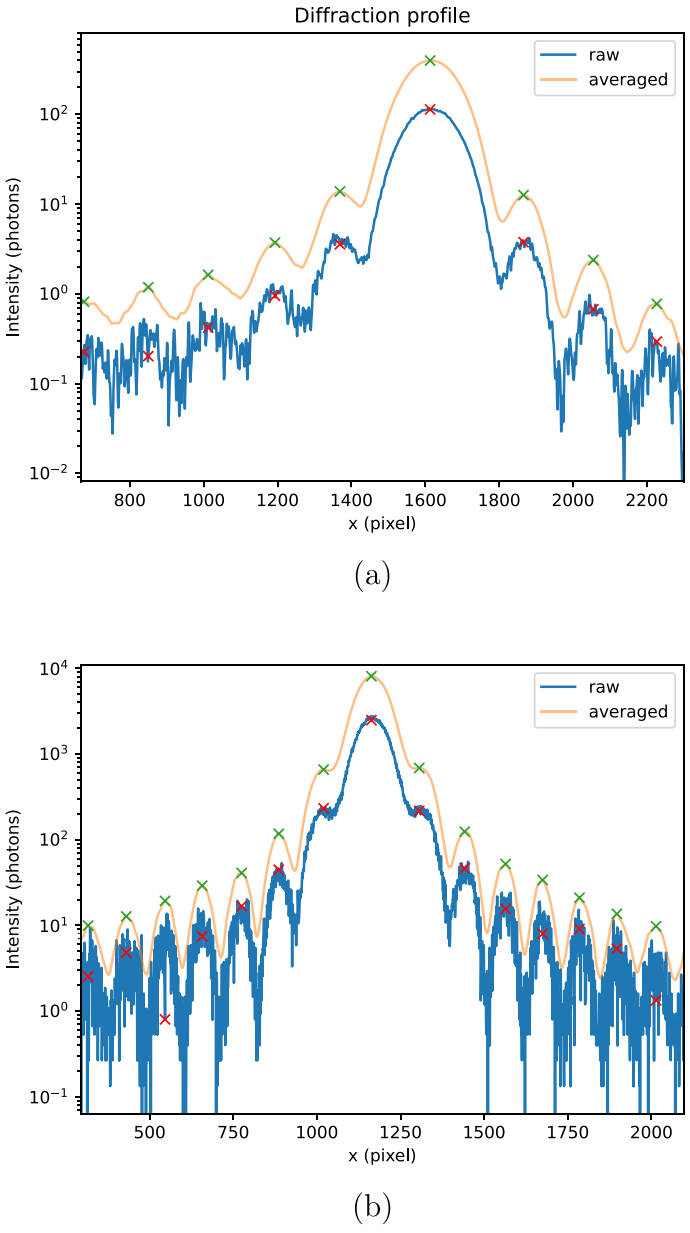

Fig. 7. Diffraction pattern for the custom intensified camera (a) and for the ORCA-Quest2 (b). In the graph, the raw data are displayed in blue; the orange line is shown to highlight the peak position and has been obtained by convoluting the data first with a binomially distributed weights, then using constant weights. The red and the green crosses are respectively the peak position on the raw and the averaged data.

However, further studies are necessary to understand whether the MCP low quantum efficiency affects the performances of the setup, despite the high amplification of the camera.

This trade-off is particularly relevant for RIPTIDE's operational conditions, where maximizing photon detection under extreme luminosity constraints is essential.

5. Conclusion

This study aimed to evaluate the performance of various optical readout systems under conditions of extreme low luminosity, a key factor for optimizing the RIPTIDE detector capability to track neutron interactions with high precision. A reliable optical system capable of resolving fine diffraction patterns in low-light environments is essential for accurate neutron energy and direction determination.

A method leveraging the well-known diffraction properties of a plane wave passing through a single slit was employed to compare the performance of three optical systems: the ASI533MM-PRO from ZWO, the ORCA-Quest2 from Hamamatsu, and an MCP-based system from PHOTEK coupled with the ASI533MM-PRO. These devices were evaluated as potential candidates for the RIPTIDE detector optical readout system, with emphasis on their ability to perform under extreme low-light conditions and at high frame rates.

The ORCA-Quest2 exhibited lower noise levels compared to the MCP setup, providing excellent photon sensitivity and clear diffraction peak resolution. However, the MCP setup allowed for the detection of lower luminosity levels due to its light amplification capabilities.

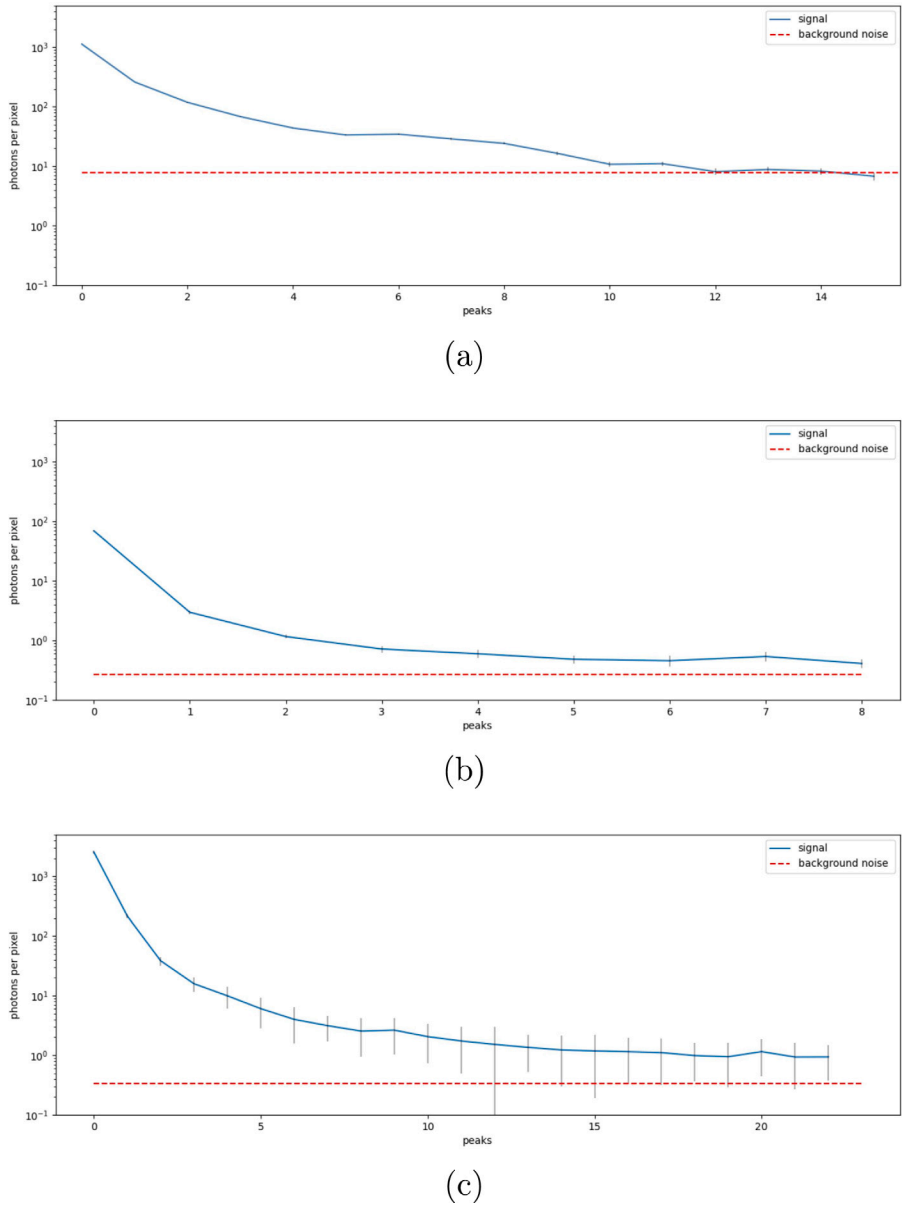

Fig. 8. Peaks photon density for the ASI533MM-PRO setup (a), custom intensified setup (b), and ORCA-Quest2 setup (c).

Despite the higher background noise associated with the MCP, its integration with a fast frame-rate camera, is better suited to RIPTIDE's requirements.

This combination enhances RIPTIDE performances, contributing to more accurate measurements of neutron energy and direction.

CRediT authorship contribution statement

Claudia Pisanti: Writing – original draft, Methodology, Investigation, Formal analysis. **Stefano Cecchini:** Supervision, Investigation. **Patrizio Console Camprini:** Supervision. **Francesco Giacomini:** Supervision. **Samuele Lanzi:** Writing – review & editing, Investigation, Formal analysis. **Cristian Massimi:** Writing – review & editing, Validation, Supervision, Investigation, Conceptualization. **Alberto Mengarelli:** Writing – review & editing, Supervision, Methodology, Investigation. **Triestino Minniti:** Writing – review & editing. **Agatino Musumarra:** Supervision. **Maria Grazia Pellegriti:** Supervision. **Alberto Piccioni:** Resources, Investigation. **Riccardo Ridolfi:** Writing – review & editing, Supervision, Methodology, Investigation. **Roberto Spighi:** Writing – review & editing, Supervision, Resources, Project administration, Funding acquisition. **Nicolas Terranova:** Validation. **Mauro Villa:** Writing – review & editing, Validation, Supervision, Investigation.

Declaration of Generative AI and AI-assisted technologies in the writing process

During the preparation of this work the authors used ChatGPT in order to clarify the sentence to improve the clarity and coherence of the writing. After using this tool, the authors reviewed and edited the content as needed and take full responsibility for the content of the published article.

Declaration of competing interest

The authors declare that they have no known competing financial interests or personal relationships that could have appeared to influence the work reported in this paper.

Data availability

Data will be made available on request.

References

ASI533-PRO MM, ZWO, 2022. URL https://www.zwoastro.com/product/asi533-pro-series/.

Bocchieri, A., et al., 2024. Scintillation event imaging with a single photon avalanche diode camera. Commun. Eng. 3 (1), 135.

Camprini, P.C., et al., 2023. A proton-recoil track imaging system for fast neutrons: the riptide detector. J. Instrum. 18 (01), C01054.

Eljen Technology, 2021. URL https://eljentechnology.com/products/plastic-scintillators/ej-200-ej-204-ej-208-ej-212.

Marafini, M., et al., 2017. Mondo: a neutron tracker for particle therapy secondary emission characterisation. Phys. Med. Biol. 62 (8), 3299.

Massimi, C., et al., 2022. riptide — an innovative recoil-proton track imaging detector. J. Instrum. (17).

Microchannel plate, PHOTEK, 2024. URL https://www.photek.com/image-intensifier/.

Mitchell, J., et al., 2024. Development of the optimized solar neutron tracking (sontrac) instrument. In: 2024 IEEE Nuclear Science Symposium (NSS), Medical Imaging Conference (MIC) and Room Temperature Semiconductor Detector Conference. RTSD, IEEE, 1–1.

Musumarra, A., et al., 2021. Riptide: a novel recoil-proton track imaging detector for fast neutrons. J. Instrum. 16 (12), C12013.

ORCA-Quest2, Hamamatsu, 2024. URL https://www.hamamatsu.com/eu/en/product/cameras/qcmos-cameras/.

Pisanti, C., et al., 2024. Riptide: a proton-recoil track imaging detector for fast neutrons. J. Instrum. 19 (02), C02074.

Potentiometer Gentec-eo, 2024. URL https://www.gentec-eo.com/products/ph100-si-ha-od1-d0.

Stoudenheimer, R., et al., 1960. Image intensifiers for nuclear track imaging. IRE Trans. Nucl. Sci. 7 (2/3), 136–141.

Tremsin, A., Vallerga, J., 2020. Unique capabilities and applications of microchannel plate (mcp) detectors with medipix/timepix readout. Radiat. Meas. 130, 106228.

Vanier, P.E., et al., 2007. Directional detection of fission-spectrum neutrons. In: 2007 IEEE Long Island Systems, Applications and Technology Conference. IEEE, pp. 1–5.

Wang, Z., Morris, C.L., 2013. Tracking fast neutrons. Nucl. Instrum. Methods Phys. Res. A 726, 145–154.

Yamamoto, S., Yoshino, M., Nakanishi, K., Yogo, K., Kamada, K., Yoshikawa, A., Kataoka, J., 2024. A comparative study of em-ccd and cmos cameras for particle ion trajectory imaging. Appl. Radiat. Isot. 204, 111143.

Yamamoto, S., et al., 2023. A high-resolution real-time imaging system for observing the trajectories of neutron induced particles in a scintillator. J. Instrum. 18 (06), T06009.